JOURNAL OF CATALYSIS 90, 337–350 (1984)

Carbon Monoxide Hydrogenation over Silica-Supported Ruthenium–Copper Bimetallic Catalysts

S. Y. LAI AND J. C. VICKERMAN

Department of Chemistry, University of Manchester Institute of Science and Technology (UMIST), Manchester M60 1QD, England

Received March 5, 1984; revised May 14, 1984

The catalytic properties of a series of ruthenium–copper catalysts supported on silica were studied. It was found that while the amount of CO adsorbed at 273 K measured with the pulse-flow method is higher on the catalysts with a small concentration of copper than on the pure ruthenium catalyst, the yield of Ru^+ secondary ions on fast atom bombardment of the catalyst surface with argon is suppressed by the addition of copper. The activity for CO disproportionation as well as CO hydrogenation were drastically reduced by the presence of copper. It is estimated that an ensemble of between 4 to 6 adjacent ruthenium atoms is required for CO disproportionation and one of between 9 to 13 adjacent ruthenium atoms is required for CO hydrogenation. Comparisons between the properties of the supported catalysts and those of single-crystal model catalysts were made.

INTRODUCTION

In recent years, much work has been done on the catalytic properties of bimetallic catalysts (*1, 2*). Among these, systems that do not form bulk alloys are of special interest. An example of these bimetallic "cluster" catalysts, the Ru–Cu system, has been examined in detail. The work of Sinfelt *et al.* (*3–6*) showed that copper interacts with ruthenium in a way similar to chemisorption, with copper adsorbed on the surface of the ruthenium-metal aggregates. The capacity for strong hydrogen and carbon monoxide chemisorption on the bimetallic catalysts is reduced compared with the pure-ruthenium catalysts (*3, 4*). While the activity of the catalysts for hydrocarbon hydrogenolysis is drastically reduced by the presence of copper, the activity for dehydrogenation is only slightly affected. In another study, Bond and Turnham found that copper greatly inhibited the methanation activity of ruthenium (*7*).

The observation that some of the ruthenium–copper bimetallic particles exhibit "raft-like" structure (*5*) initiated detailed studies of well-characterized ruthenium–copper model catalysts prepared by evaporation of copper onto a ruthenium (0001) single-crystal surface (*8–12*). It was observed that the structure of the copper overlayer depends on the deposition temperature. Copper is adsorbed on ruthenium with a binding energy ca. 16 kJ mol^{-1} larger than the sublimation energy of copper. With sufficient thermal energy (deposition at 1080 K), copper spreads on the ruthenium surface in a predominantly two-dimensional fashion below a copper coverage of one monolayer. At very low copper coverage, the existence of isolated copper atoms was postulated. When the deposition temperature was low (540 K), small copper clusters formed at low coverage and three-dimensional copper aggregates started to form before the first monolayer was completed. Adsorption studies showed that strongly adsorbed CO on pure-ruthenium sites was greatly reduced by the presence of copper. An ensemble size of about 3 Ru atoms is required for strong CO adsorption. When the adsorption temperature was lowered from 320 to 150 K, adsorption on sites with energy intermediate between that of

0021-9517/84 $3.00

pure ruthenium and copper was observed. These were assigned to adsorption on mixed ruthenium–copper sites as well as isolated copper sites. The total CO coverage on the bimetallic surface increased and the effect was more pronounced on the surfaces prepared at low temperature (*10*). Similarly, hydrogen adsorption on ruthenium was inhibited by copper (*9*). However, on the high-temperature series at very low coverage ($\theta_{Cu} \leq 0.05$) an enhancement of D_2 adsorption on ruthenium sites was observed (*11*). An electronic effect due to isolated copper atoms was proposed.

In view of these findings, it is interesting to study the behaviour of "real" supported ruthenium–copper catalysts to observe if a correspondence with the model catalysts exists and to observe the consequences these variations in adsorptive properties have on the catalytic activity and selectivity for CO hydrogenation.

This paper reports on the study of a series of ruthenium–copper bimetallic catalysts supported on high-surface-area silica. Their activities in CO adsorption, CO disproportionation and CO hydrogenation were examined.

EXPERIMENTAL

Catalyst Preparation

The catalysts were prepared by coimpregnation. Aqueous solutions of $RuCl_3 \cdot H_2O$ and $Cu(NO_3)_2 \cdot 3H_2O$ mixed in appropriate proportions and acidified by dilute HCl to maintain the $RuCl_3$ in solution were mixed with silica gel. The slurries were stirred vigorously for 30 min and then dried at 383 K for more than 15 h. The dried powders were then reduced in flowing hydrogen at 723 K for ca. 15 h. The compositions of the catalysts were determined by atomic absorption and are shown in Table 1. The catalysts are designated as RC/x:y where x:y is the ruthenium : copper ratio on the samples.

TABLE 1

Composition of the Ruthenium–Copper Catalysts

Sample designation	Ru loadings % (w/w)	Cu loadings % (w/w)	Cu/Ru atomic ratio (%)
RC/100:0	0.88	—	0.0
RC/100:2	0.84	0.010	1.9
RC/100:5	0.76	0.026	5.4
RC/100:9	0.93	0.050	8.6
RC/100:16	0.74	0.073	15.7
RC/100:33	0.78	0.160	32.6

Fast Atom Bombardment—Mass Spectrometry (FABMS)

The surface concentration of ruthenium and copper on the catalysts were examined with a Vacuum Generators Secondary Ion Mass Spectrometer—Fast Atom Bombardment Spectrometer. Prior to the analysis, the catalyst powders were sputtered with an argon ion beam with an ion current of 20 μA for 7 min to remove hydrocarbons adsorbed on the catalyst surface. The positive secondary ions generated on bombardment with a fast argon atom beam were measured using a VG MM 12-12 quadrupole mass spectrometer.

Transmission Electron Microscopy

Catalyst samples suitable for examination with transmission electron microscopy were prepared by grinding the catalysts into very fine powders which were then dispersed in acetone. A drop of suspension was transferred onto a holey carbon film supported on a copper grid. The samples were dried in air and then examined using a Philips EM 400T transmission electron microscope equipped with X-ray analytical facilities.

CO Adsorption and Disproportionation

CO adsorption and decomposition were performed in a pulse-flow reactor system. The reactor was a 5-mm-i.d. Pyrex glass U-tube. For each run ca. 0.5 g of catalyst was used and held in the reactor with plugs of glass wool. Prior to the adsorption or dis-

proportionation experiments, the catalyst was reduced *in situ* by flowing hydrogen at 723 K for 30 min. The reactor was then purged with helium at 723 K to remove any adsorbed hydrogen and then cooled slowly to the required temperature. For the adsorption experiments, the reactor was held at 273 K with an ice bath and pulses of CO gas (0.16 cm^3) were passed over the catalyst until the areas of the eluted peaks were constant. The quantity of CO uptake was calculated as the difference of the volume of CO injected and eluted.

In the CO disproportionation experiment, the reactor was held at 573 K inside a ventilated furnace. Ten pulses of CO (0.16 cm^3) were passed over the catalyst bed. H_2 was then passed over the catalyst surface to hydrogenate the surface carbon species. A Poropak N column was placed downstream of the reactor to separate the CO, CO_2, H_2, and hydrocarbon. A katharometer was used for gas detection.

Hydrogen and helium gases used were purified by liquid-nitrogen cold traps to remove condensable impurities. CO gas was first passed through a solid KOH trap to remove traces of CO_2 and then through a molecular-sieve trap to remove H_2O.

CO Hydrogenation

CO hydrogenation experiments were performed in a single-pass flow reactor system. The reactor was made of 1-cm-i.d. silica tube with a sintered silica disk supporting the catalyst bed. The temperature of the catalyst was measured with a Chromel–Alumel thermocouple placed in a thermocouple well inside the catalyst bed. A premixed gas with composition 10.45% CO: 47.40% H_2: 42.15% Ar (v/v/v) was used as the reactant. In each catalytic run, ca. 0.3 g of the catalyst was used. Each fresh sample was pretreated *in situ* with flowing hydrogen at 723 K for 30 min. The catalyst was then cooled to the reaction temperature and the hydrogen replaced by the reactant gas mixture. Two Pye 104 gas chromatographs, one with a flame ionisation detector and silica gel column to detect hydrocarbon and the other with a katharometer and molecular sieve 5A column to detect hydrogen and carbon monoxide were used for product analysis. After each kinetic run, the catalyst was heated in hydrogen at 723 K for 1 to 2 h until no hydrocarbons could be detected at the reactor outlet. The activity of the catalyst 30 min after the reactant was introduced was measured and taken to represent the initial activity. Since the reaction is highly exothermic with a heat of reaction (ΔH) per carbon of 214 kJ mol^{-1} for the formation of methane, the conversion was kept as low as possible and did not exceed 5% in all the experiments. The temperature of the catalyst bed was closely monitored and no overheating was observed.

RESULTS AND DISCUSSION

Fast Atom Bombardment–Mass Spectrometry

In FABMS, the yield of secondary ion is sensitive to slight variations of the experimental conditions. To allow meaningful comparisons of surface concentration to be made from sample to sample, a signal from the support material (Si_2O^+, mass 72) was used as an internal standard. The variations of the secondary ion yield of ruthenium (expressed as the intensity ratio $^{102}Ru^+$/

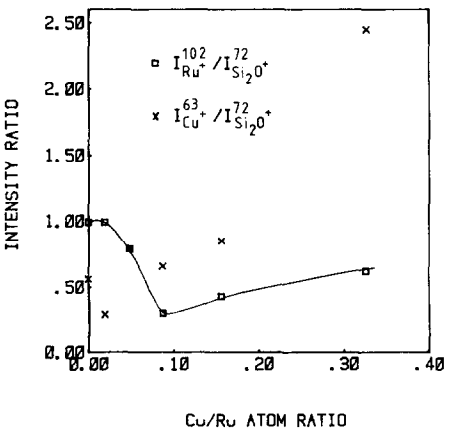

FIG. 1. Plot of the secondary ion intensity ratios as a function of the composition of the SiO_2-supported catalysts.

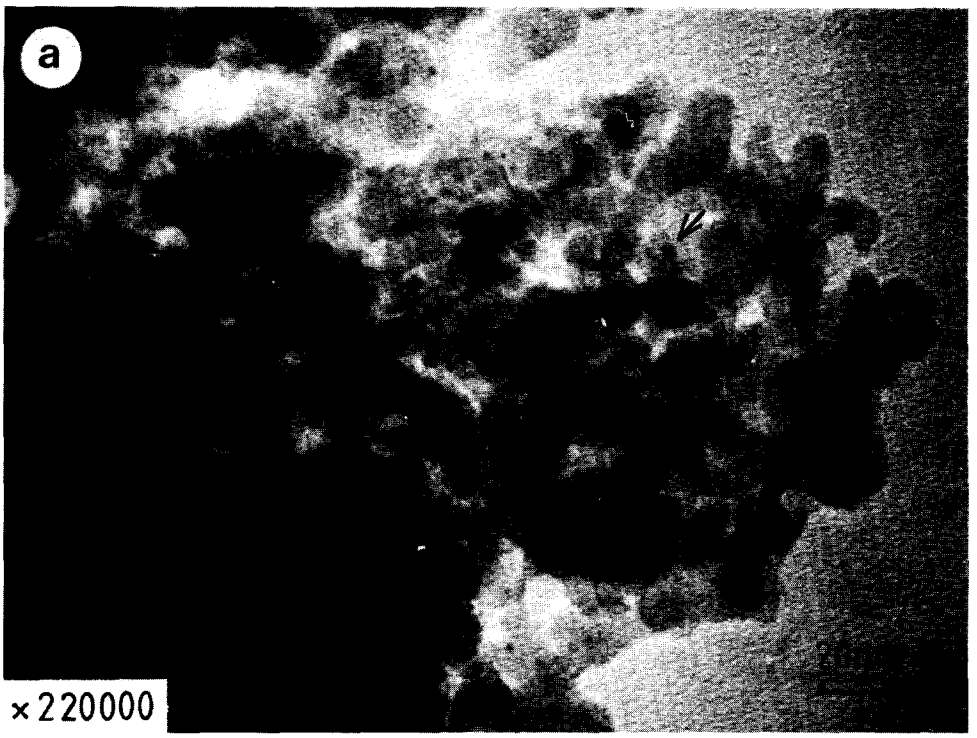

FIG. 2. Transmission Electron Micrographs of the catalysts. (a) RC/100 : 0. The samples RC/100 : 2, RC/100 : 5, and RC/100 : 9 have similar particle size distribution. (b) RC/100 : 16. Different areas of this sample show very different particle size distribution. The result for metal dispersion calculated is probably too low since the larger particles are more likely to be observed and measured. (c) RC/100 : 33.

$^{72}Si_2O^+$) and copper ($^{63}Cu^+/^{72}Si_2O^+$) are shown in Fig. 1. It was found that the hydrocarbon contamination could not be completely removed by the sputter cleaning procedure. The secondary ion signal at mass 63 contained a significant contribution from hydrocarbon fragments and hence the measured Cu/Si_2O ratio is subject to some uncertainty. The signal at mass 102 was relatively free from interference from the hydrocarbons. Figure 1 shows that the intensity ratio Ru^+/Si_2O^+ was suppressed with the addition of copper to the catalysts. This is clear confirmation of the suggestion by Sinfelt *et al.* (*3, 6*) that copper and ruthenium form bimetallic crystallites with copper preferentially segregated on the surface. At a copper–ruthenium ratio of above 10%, increase of copper did not cause further reduction of the ruthenium secondary ion yield, possibly suggesting the formation of three-dimensional copper aggregates. In addition, results from experiments with ruthenium having different dispersions indicate that emission of secondary ions as a proportion of the number of atoms which are surface atoms increases with increasing particle size. Results from transmission electron microscopy (see next section) show that the samples RC/100 : 16 and RC/100 : 33 have larger average particle diameter than the other catalysts. This may have an effect on the secondary ion yield for these two catalysts also.

Static Secondary Ion Mass Spectrometry studies using single-crystal models showed that the presence of copper significantly affects the Ru^+ ion yield (*12*). As for the "real" powder catalysts studied in the present case, the effects of hydrocarbon

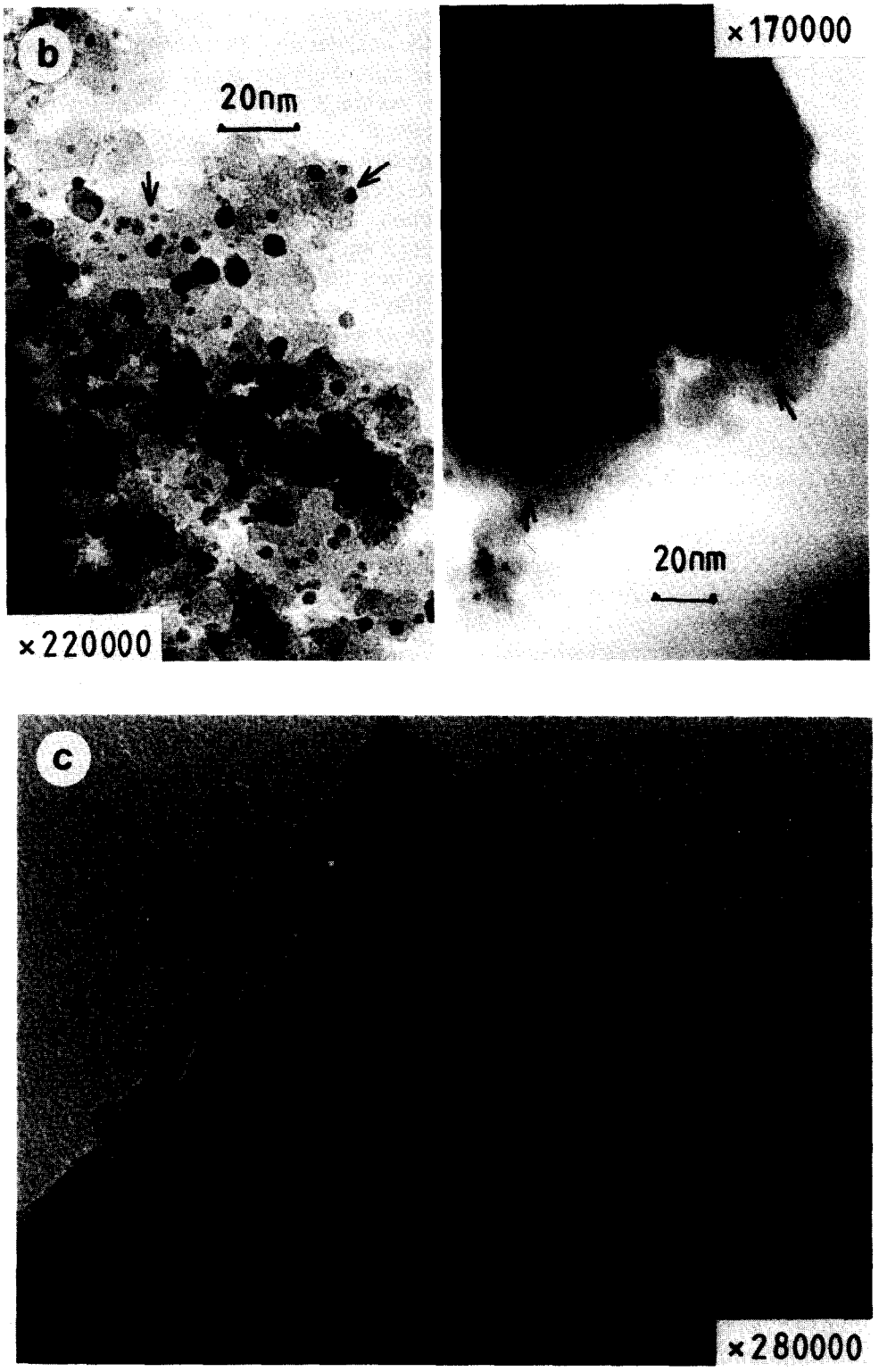

FIG. 2—*Continued.*

contaminants and the location of the metal aggregates, whether they are on the outer surface or inside the pores and channels of the support particles, present further complications. With so many variables that are not easily quantifiable, the use of the FABMS data for the accurate estimation of the metal coverage on the catalyst surface is not really feasible.

Transmission Electron Microscopy

TEM has been used widely for studying supported metal catalysts (*13*). The structure and size distribution of the metal particles can often be observed. With additional analytical attachments, the local composition of different areas on a specimen can be determined.

Some representative electron micrographs of the catalyst samples taken with 100 kV electron energy and magnification of ×220,000 are shown in Fig. 2. More or less circular particles showing high contrast are readily discernable from the background of the support material. These particles were shown to contain ruthenium by analyzing the X rays generated on electron impact. The presence of copper could not be confirmed because a larger copper signal was always observed due to the excitation of the copper grid by stray secondary electrons and X rays generated from the sample. The size of the particles was measured and are presented as size distribution graphs (Fig. 3). Assuming a spherical shape, the total metal dispersion was calculated using the equation

$$\text{Dispersion}(\%) = \frac{6\Sigma f_i d_i^2 V}{\Sigma f_i d_i^3 A} \cdot 100.$$

where

f_i = number of particles of diameter d_i,

V = effective volume of a metal atom,

A = effective cross sectional area of a metal atom.

A surface ruthenium density of 1.63×10^{19} atoms m^{-2} (*14*) and a bulk ruthenium density of 1.24×10^7 g m^{-3} (*15*) were used in the calculation. The effect of the difference in size of copper atoms was ignored.

Although TEM allows the catalyst particles to be observed directly, its use as a quantitative tool has some limitations. Due to accidental alignment of atoms, the amorphous support exhibits a speckled appearance and metal particles smaller than 5 Å cannot be distinguished from the support. Only a very small area of the catalyst sample is displayed in each micrograph. When only a small number of electron micrographs are available, a large sampling error can occur, especially in the case of samples with uneven particle size distribution. For representative sampling to be achieved, more than a thousand particles from at least a few different preparations must be measured. Such conditions could not be satisfied in the present case. The metal dispersion calculated is therefore only a qualitative measure of the state of dispersion of the catalyst samples.

In order to compare the behavior of the supported catalysts with the single crystal models (*8–11*), the catalyst should be well characterised. Ideally, the total metal dispersion as well as the distribution of both components should be known. However, for this series of catalysts, apart from FABMS and transmission electron microscopy other commonly used methods for characterisation could not be applied successfully. Because of the low metal loading and small particle size, no X-ray diffraction lines from the individual metals could be detected. Results from adsorption studies on the model catalysts showed that the chemisorptive capacity of the bimetallic catalysts for CO and H_2 do not vary linearly with the surface concentration of the active metal (*9, 11*). Chemisorption experiments cannot therefore provide information about the ruthenium dispersion either.

Using FABMS, the formation of bimetallic clusters is demonstrated. However, quantitative measures of the coverage of copper on ruthenium cannot be made. In

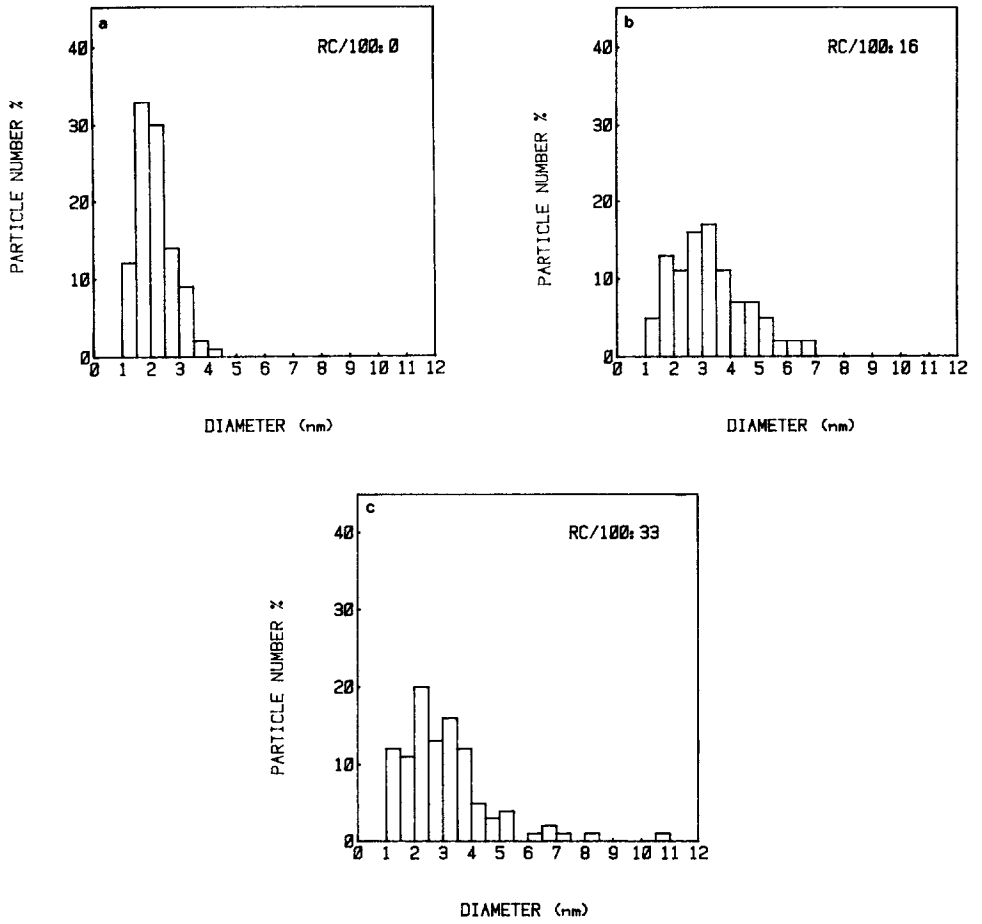

FIG. 3. Particle size distribution of the catalysts.

the absence of more accurate information, the copper coverage of the catalysts are estimated using the total metal dispersion calculated from TEM and assuming all copper atoms to be present as a monolayer on the metal particle surface (Table 2). With all the inherent uncertainties in the assumptions involved, the θ_{Cu} values so obtained should only be taken as a qualitative trend rather than quantitatively.

Carbon Monoxide Adsorption

The application of the dynamic-pulse method for adsorption studies has been described in detail in the literature (*17–20*). It was argued that for *strong irreversible chemisorption,* the total quantity of gas adsorbed can be found by measuring the difference between the quantity of gas in-

TABLE 2

Metal Dispersion in the Catalysts

Sample	Number average particle diameter (nm)	Metal dispersion (%)	Copper coverage[a]
RC/100:0	2.2	52	0.0
RC/100:2	2.1	53	0.04
RC/100:5	2.1	55	0.09
RC/100:9	1.8	63	0.13
RC/100:16	3.3	31	0.44
RC/100:33	3.4	27	0.91

[a] Estimated with the assumption that copper occurs as a monatomic layer on the surface.

jected and the quantity of gas eluted. The results of CO uptake by the Ru–Cu catalysts are presented in Table 3 and Fig. 4.

The observation that CO uptake is higher on the bimetallic catalysts than on pure ruthenium is apparently surprising and seems to contradict the results of Sinfelt *et al.* (*3, 4*). To understand this it is useful to compare it with the result of the single-crystal system (*10*). Figure 7 of Ref. (*10*) showed that when equilibrated at 150 K, in the ultrahigh vacuum system, copper atoms themselves constitute sites for CO adsorption and are probably involved in mixed Cu–Ru sites. While the temperature used in the pulse-flow experiment was 273 K, much higher than in the UHV experiment, a comparison between the two experiments is not unjustifiable. From the area and height of the eluted peak, the maximum pressure of CO at the end of the catalyst column was estimated to be about 2500 Pa, seven orders of magnitude higher than that used in the UHV system. Under this high pressure, adsorption on the weak Cu or Cu–Ru sites would have occurred and the slow desorption from these sites would not be completed in the time interval between successive injections. Therefore, with the pulse-flow method, it is very likely that at least part of CO adsorbed on sites associated with copper was measured. Recently, Sarkany and Gonzalez have discussed the difficulties in using the pulse method for measuring metal surface area when slow reversible processes take place (*20*). The results obtained in this study again show the problem in interpreting the results of pulse-flow adsorption experiments when adsorption on sites of a range of different energies is involved. Nevertheless, the results shown in Table 3 indicate that on the bimetallic surface, copper is active in creating CO adsorption sites, in agreement with the work on the model catalysts.

TABLE 3

CO Uptake of the Ruthenium–Copper Catalysts Measured at 273 K with the Pulse-Flow Method

Sample	CO uptake ($cm^3\ g^{-1}$ (STP))	CO/Ru
RC/100:0	0.31	0.16
RC/100:2	0.36	0.19
RC/100:5	0.35	0.21
RC/100:9	0.45	0.22
RC/100:16	0.35	0.22
RC/100:33	0.31	0.18

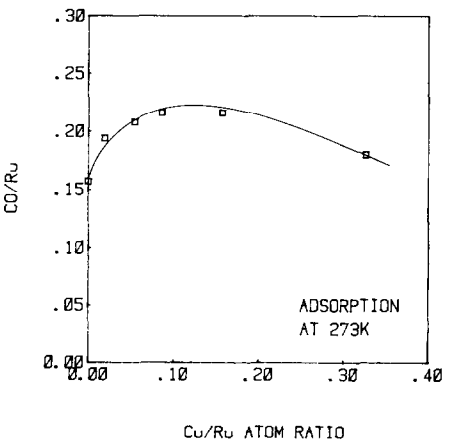

FIG. 4. The effect of copper on CO adsorption.

CO Disproportionation

The role of metal carbides in the Fischer–Tropsch synthesis has been the subject of many studies (*22, 23*). The work of Wentrcek *et al.* (*24*) an Araki and Ponec (*26*) indicated that carbon deposited onto Ni by CO disproportionation at temperatures commonly encountered in Fischer–Tropsch synthesis was active in producing methane on hydrogenation. Work by Low and Bell (*25*) and Biloen *et al.* (*27*) has shown that such surface "carbidic" species on ruthenium were also active towards hydrogenation. To investigate the role of dissociated carbon in the Fischer–Tropsch synthesis, it would be useful to observe the effect of copper on the activity of ruthenium for both CO disproportionation and CO hydrogenation.

On passing CO over the catalysts at 573 K, carbon dioxide was produced. The quantity of carbon deposited on the catalyst was calculated assuming that the reaction proceeds as

$$2CO \rightarrow C_{ads} + CO_2. \quad (1)$$

It was found that less than 10 pulses of CO were sufficient to saturate the catalyst surface for all the samples. When hydrogen was pulsed over the catalysts, methane, together with small quantities of ethane, was formed. The quantity of carbon deposited and the hydrocarbon yield are given in Table 4. The mass balance for the carbon in the disproportionation as calculated from Eq. (1) was found to be less than 100% in most cases. Gaustafson and Lunsford (*28*) have argued that on a RuY zeolite catalyst at 573 K, reaction is possible according to

$$CO \rightarrow C_{ads} + O_{ads}. \quad (2)$$

The amount of carbon deposited could be higher than that estimated with Eq. (1). On the other hand, the quantities of carbon removed by hydrogenation were less than that of deposited carbon. Conversion of the "carbidic" carbon into an inactive form could have taken place. It is therefore felt that the quantity of carbon capable of being hydrogenated is a better measure of the capacity of the catalysts in adsorbing "active carbon." Figure 5 shows that unlike CO adsorption, CO disproportionation is markedly suppressed by copper, in a similar manner to strong CO adsorption on pure ruthenium sites (*10*).

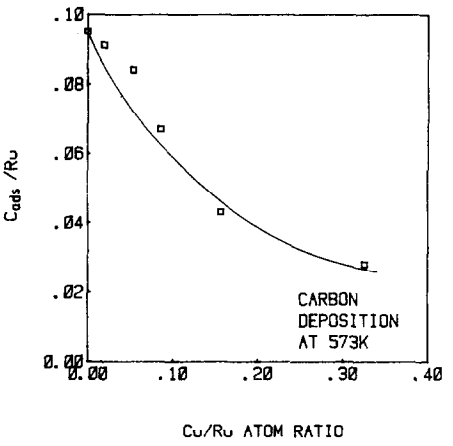

FIG. 5. The effect of copper on CO disproportionation.

CO Hydrogenation

The activity of the catalysts in CO hydrogenation is shown in the form of the Arrhenius plots in Fig. 6. From the curves, it is obvious that the activity of ruthenium is reduced by copper. An increase in the apparent activation energy (Table 5) as copper is added to the ruthenium is also observed, indicating that copper exerts an electronic effect on ruthenium. The work of Vannice (*29*) established that a compensation effect exists for different Group VIII metals for this reaction. Comparing the activity of samples RC/100:0 and RC/100:2 reveals that while the apparent activation energy is

TABLE 4

CO Disproportionation at 573 K

Sample	Carbon deposited (mol g^{-1})	CH_4 produced (mol g^{-1})	C_2H_6 produced (mol g^{-1})	C_{ads}/Ru^a
RC/100:0	1.29×10^{-5}	7.80×10^{-6}	2.61×10^{-7}	0.095
RC/100:2	1.15×10^{-5}	7.06×10^{-6}	2.60×10^{-7}	0.091
RC/100:5	8.22×10^{-6}	6.33×10^{-6}	0	0.084
RC/100:9	6.06×10^{-6}	6.16×10^{-6}	0	0.067
RC/100:16	6.56×10^{-6}	3.17×10^{-6}	0	0.043
RC/100:33	3.20×10^{-6}	2.12×10^{-6}	0	0.028

[a] Carbon which can be hydrogenated.

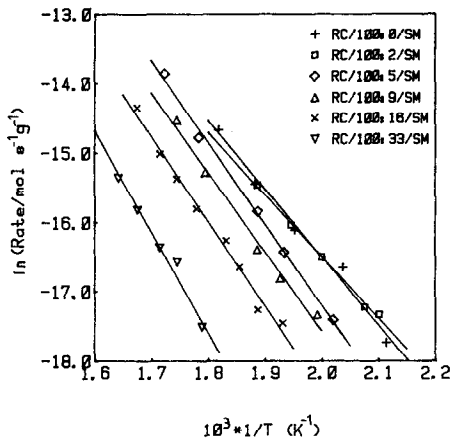

FIG. 6. Arrhenius plots for CO hydrogenation on the ruthenium–copper catalysts.

substantially different, the reaction rates at 480–530 K for both catalysts are similar. For this temperature range, the effect of the variation of the entropy contribution to the preexponential factor and the activation energy have cancelled each other out and the effect of copper in blocking the active sites for the reaction should predominate. In the following discussion, the activity and selectivity of the catalysts at 530 K are compared.

The mechanism of the Fischer–Tropsch reaction has been the subject of many reviews (*30–34*) and many recent studies (*35–46*). The nature of the elementary steps has not as yet been settled conclusively. The details of the mechanism probably vary with both the nature of the catalyst and the reaction conditions. The kinetics of the reaction over Group VIII metals are consistent with a scheme in which the rate-determining step involves the reaction of a species derived from carbon monoxide and adsorbed hydrogen (*31*). One possible sequence of steps leading to the formation of hydrocarbon is postulated as

$$CO(g) + S \leftrightarrow CO_{ads} \quad (3)$$

$$H_2(g) + 2S \leftrightarrow 2H_{ads} \quad (4)$$

$$CO_{ads} + S \rightarrow C_{ads} + O_{ads} \quad (5)$$

$$2H_{ads} + O_{ads} \rightarrow H_2O + 3S \quad (6)$$

$$C_{ads} + nH_{ads} \rightarrow CH_{n\,ads} + nS \quad (7)$$

$$CH_{n\,ads} \rightarrow \text{hydrocarbons} \quad (8)$$

where S is a vacant surface active site. If step (7) is the rate-determining step, then the rate of CO hydrogenation would be

$$\text{rate} = k_7\theta_C\theta_H^n.$$

Any effect of copper on the adsorption of hydrogen and "active" carbon will lead to a parallel change in the CO hydrogenation activity.

In Fig. 7a, the curve of the relative rate of hydrogenation activity as a function of the ruthenium coverage, together with the curve for the relative capacity of CO disproportionation are plotted. The parallel between the two curves and their similarity to the behaviour of strong CO and hydrogen adsorption on the single crystals is apparent (*10, 11*). The parallel between the effects of copper on CO disproportionation and CO hydrogenation suggests that the two processes proceed via the same reaction intermediate. A similar conclusion was arrived at by Rostrup-Nielsen and Pedersen, who studied the effect of sulphur poisoning on nickel and found no change in the selectivity for the Boudouard reaction and methanation reaction (*50*). This is consistent with the proposition that CO hydrogenation proceeds via CO dissociation. From the slope of the curves at small θ_{Cu}, the number of neighbouring ruthenium atoms required for CO disproportionation and CO

TABLE 5

Apparent Activation Energies of the Catalysts for CO Hydrogenation

Sample	Apparent activation energy (kJ mol^{-1})
RC/100:0	82 ± 13
RC/100:2	73 ± 4
RC/100:5	97 ± 8
RC/100:9	95 ± 14
RC/100:16	101 ± 9
RC/100:33	121 ± 12

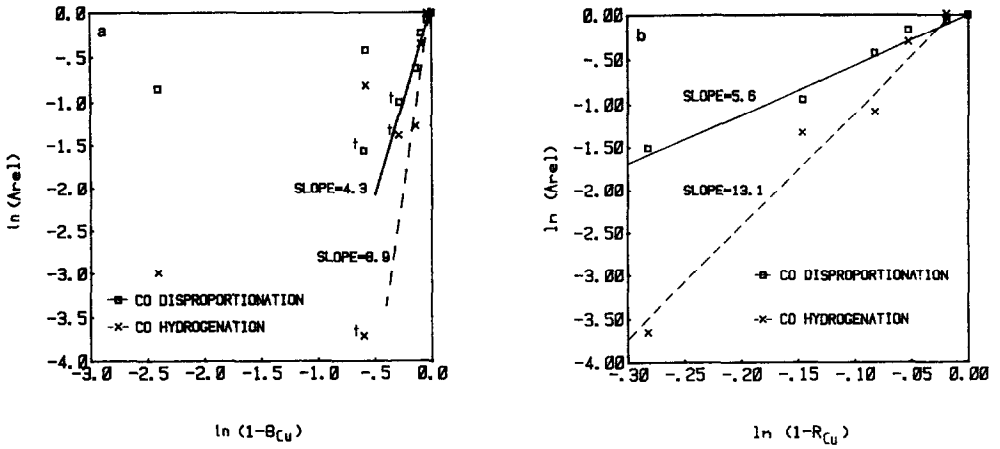

FIG. 7 (a) The relative activity of the catalysts as a function of copper coverage. † Due to the uncertainty in estimating the metal dispersion for the samples RC/100 : 16 and RC/100 : 33, the relative activity of these two catalysts are also calculated by assuming that they have a metal dispersion of 55%, similar to the other samples, and the data plotted for comparison. (b) The relative activity of the catalysts as a function of the bulk copper to total metal atom ratio.

hydrogenation was estimated to be about 4 and 9, respectively. At higher θ_{Cu}, the decrease in activity is much smaller, suggesting the formation of two-dimensional islands and three-dimensional clusters of copper. However, inspection of Fig. 3 shows that for the two catalyst samples with higher copper loading, the particle size distribution is much wider than the other samples. As a result, a larger sampling error is likely. It is therefore difficult to infer whether the decrease in the slopes of the curves is a result of a real physical structural effect or a result of the error in estimating the metal dispersion.

As discussed in the section on TEM, the calculated θ_{Cu} values are only qualitative estimates. By assuming a structure with minimum possible surface to volume ratio for the ruthenium particles and ignoring three-dimensional cluster formation for copper, θ_{Cu} would possibly be overestimated. At the other extreme, if it is assumed that all the metal atoms occur as a monolayer with copper and ruthenium randomly distributed, θ_{Cu} is given by $1/(1 + 1/r)$, where r is the bulk Cu/Ru ratio. The ensemble size thus calculated (Fig. 7b) is 6 and 13 for CO disproportionation and hydrogenation, respectively. By assuming maximum dispersion for the metals, the calculated θ_{Cu} should be an underestimate. The actual ensemble size for CO disproportionation probably lies between 4 and 6 ruthenium atoms and that for CO hydrogenation 9 to 13. The ensemble size for CO hydrogenation is about 2 to 3 times that for CO disproportionation. Since an ensemble of 4 to 6 Ru atoms is required for H_2 adsorption (*11*), this can be envisaged if the rate-determining step of the reaction requires an adsorbed carbon and one or more adsorbed hydrogen atoms arranged adjacent to each other. Studies on other bimetallic systems (e.g., Ni–Cu) also revealed that a large ensemble of active metal atoms is required for CO hydrogenation. Dalmon and Martin (*51*) found that on Ni–Cu alloys, the ensemble size for methanation is 12 Ni atoms.

An interesting change in the selectivity of the reaction with copper coverage is also observed (Fig. 8). Under the conditions of most Fischer–Tropsch syntheses, the relative concentration of paraffins and olefins is far from that predicted by thermodynamics, indicating that the reaction is kinetically controlled. If secondary reactions are ignored, the formation of paraffins and olefins

can be described as two competing reactions.

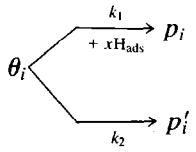

θ_i = adsorbed intermediates with i carbon atoms

p_i = paraffin formed from θ_i

p_i' = olefin formed from θ_i

The ratio of paraffin to olefin will follow the equation

$$\frac{Np_i}{Np_i'} = \frac{k_1}{k_2}\theta_H^x$$

If the rate constants k_1 and k_2 remain unchanged with copper coverage, then the ratio of the conversion to paraffins and olefins is a measure of the concentration of adsorbed hydrogen on the catalysts. Figure 8 shows that while adsorption of hydrogen is inhibited at high copper coverage, it is enhanced at low copper coverage. Similar phenomena have been observed for the model catalysts with copper deposited at 1080 K (*11*). Apart from the promoting effect of isolated copper atoms by increasing the charge density on adjacent ruthenium atoms, the reduction in binding energy of CO on ruthenium could also permit hydrogen to compete more successfully for ruthenium sites. The increase in selectivity for methane with increasing copper coverage is consistent with the observation by Bond and Turnham (*7*).

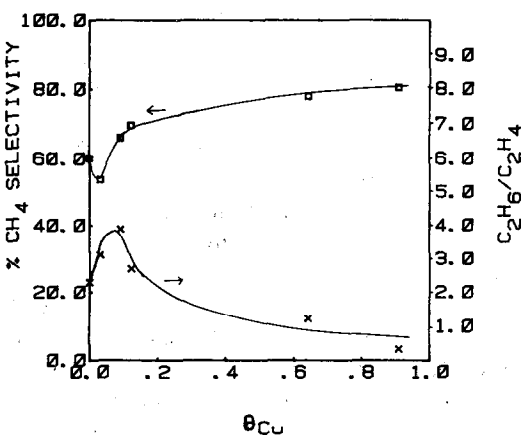

FIG. 8. The effect of copper on the selectivity of the catalysts for CO hydrogenation.

At this point it is useful to summarise the similarities in behaviour between the "real" catalysts and the "model" catalysts.

(1) The total capacity for CO adsorption on both systems is increased by a low surface coverage of copper.

(2) The quantity of hydrogen adsorbed on both systems is reduced by a moderate to high coverage of copper. At very low copper coverage when the existence of isolated copper atoms is possible, the adsorption of hydrogen is increased.

Although the conditions under which the "real" catalysts and the "model" catalysts were studied were very different, the qualitative similarities between the systems are remarkable. This suggests a possible similarity between the structure of the two systems. While the structure of the model catalysts is relatively well defined, that of the dispersed catalysts can only be speculated upon. If, as suggested by Prestridge *et al.* (*5*), the metal particles exist in thin "raft-like" structures, the exposed surface will very probably be the hexagonal (0001) face, since this offers the highest degree of coordination for the surface atoms. This structure would be similar to that of the "model" catalysts except for a larger increase in the proportion of edge atoms. A similarity in behaviour between the two can be expected if the edge atoms do not form sites with different activity. On the other hand, if, as suggested by Romanowski (*52*), the equilibrium structure for small metal particles of metal with hexagonal close-packed crystal structure is either a hexagonal column or a hexagonal truncated bipyr-

amid, then apart from the presence of highly coordinatively unsaturated corner and edge atoms, faces with orientations other than (0001) should also be exposed. A similarity in behaviour between the "model" and "real" systems will require the adsorptive properties of ruthenium and the effect of copper on them to be similar on different crystal faces. Further work on single-crystal faces with different orientations and various concentrations of crystal imperfections should shed more light on this problem.

The mechanism by which catalysts work cannot be completely understood until the relationship between the catalyst structure and its catalytic properties is elucidated. However, for highly dispersed catalysts, structural characterisation is often difficult. The study of massive "models" of single-crystal samples is attractive since these samples can be examined with various surface analytical techniques. The usefulness of this approach lies in how closely the "models" can be made to resemble the "real" catalysts in structure. By its nature, no one single-crystal system can be an adequate model for a highly heterogeneous "real" catalyst. However, by studying different types of single-crystal faces, each having some similarities to part of the "real" catalysts, the ultimate aim of uncovering the way catalysts work may be approached.

CONCLUSION

1. The behaviour of the supported ruthenium–copper catalysts corresponds well with that of the single-crystal models.

2. Weakly bonded CO on mixed ruthenium–copper sites does not take part in CO disproportionation or CO hydrogenation.

3. Between 4 and 6 adjacent ruthenium atoms are required for CO disproportionation and between 9 and 13 for CO hydrogenation.

ACKNOWLEDGMENTS

The authors thank Mr. I. Brough, Mr. G. Cliff and Mr. P. Kenway of the Metallurgy Department, UMIST, for their help in the TEM work. We also thank Johnson Matthey Chemicals Limited for supplying the ruthenium trichloride for the catalyst preparation. S. Y. Lai gratefully acknowledges the financial assistance from the British Council for her work at UMIST.

REFERENCES

1. Clarke, J. K. A., *Chem. Rev.* **75**(3), 291 (1975).
2. Moss, R. L., *Catalysis (London)* **1,** 37 (1977).
3. Sinfelt, J. H., *J. Catal.* **29,** 308 (1973).
4. Sinfelt, J. H., Lam, Y. L., Cusumano, J. A., and Barnett, A. E., *J. Catal.* **42,** 227 (1976).
5. Prestridge, E. B., Via, G. H., and Sinfelt, J. H., *J. Catal.* **50,** 115 (1977).
6. Helms, C. R., and Sinfelt, J. H., *Surf. Sci.* **72,** 229 (1978).
7. Bond, G. C., and Turnham, B. D., *J. Catal.* **45,** 128 (1976).
8. Christmann, K., Ertl, G., and Shimizu, H., *J. Catal.* **61,** 412 (1980).
9. Shimizu, H., Christmann, K., and Ertl, G., *J. Catal.* **61,** 412 (1980).
10. Vickerman, J. C., Christmann, K., and Ertl, G., *J. Catal.* **71,** 175 (1981).
11. Vickerman, J. C., and Christmann, K., *Surf. Sci.* **120,** 1 (1982).
12. Brown, A., and Vickerman, J. C., *Surf. Sci.* **140,** 261 (1984).
13. Schmidt, L. D., Wang, T., and Vacquez, A., *Ultramicroscopy* **8,** (1–2) 175 (1982).
14. Anderson, J. R., "Structure of Metallic Catalysts." Academic Press, New York, 1975.
15. "Handbook of Physics and Chemistry" (R. C. Wear, Ed.). CRC Press, Boca Raton, Fla., 1973.
16. Grubr, H. L., *Anal. Chem.* **34,** 1828 (1962).
17. Roca, F. F., de Mourgues, L., and Trambouze, Y., *J. Gas Chromatogr.* **6,** 161 (1968).
18. Freel, J., *J. Catal.* **25,** 139 (1972).
19. Eberly, P. E., *J. Phys. Chem.* **65,** 68 (1961).
20. Sarkany, J., and Gonzalez, R., *J. Catal.* **76,** 75 (1982).
21. Pilcher, H., "Advances in Catalysis," Vol. 4, p. 271. Academic Press, New York, 1952.
22. Fischer, F., and Tropsch, H., *Ber. Dtsch. Chem. Ges. B* **59,** 830 (1926).
23. Kummer, J. T., de Witt, T. W., and Emmett, P. H., *J. Amer. Chem. Soc.* **70,** 3632 (1948).
24. Wentrcek, P. R., Wood, B. J., and Wise, H., *J. Catal.* **43,** 363 (1976).
25. Low, G. G., and Bell, A. T., *J. Catal.* **57,** 397 (1979).
26. Araki, M., and Ponec, V., *J. Catal.* **44,** 439 (1976).
27. Biloen, P., Helle, J. N., and Sachtler, W. M. H., *J. Catal.* **58,** 95 (1979).

28. Gustafson, B. L., and Lunsford, J. H., *J. Catal.* **74,** 393 (1982).
29. Vannice, M. A., *J. Catal.* **37,** 462 (1975).
30. Mills, G. A., and Steffgen, F. W., *Catal. Rev.* **8,** 159 (1973).
31. Vannice, M. A., *Catal. Rev.* **14,** 153 (1976).
32. Biloen, P., and Sachtler, W. M. H., "Advances in Catalysis," Vol. 30, p. 165. Academic Press, New York, 1981.
33. Kelley, R. D., and Goodman, D. W., *in* "The Chemical Physics of Solid Surface and Heterogeneous Catalysis" (D. A. King and D. P. Woodruff, Ed.). Elsevier, Amsterdam, 1982.
34. Rofer-De Poorter, C. K., *Chem. Rev.* **81,** 447 (1981).
35. Kellner, C. S., and Bell, A. T., *J. Catal.* **67,** 175 (1981).
36. Pradeep, K., Agrawal, P. K., Katzer, J. R., and Manogue, W. H., *J. Catal.* **69,** 327 (1981).
37. Cant, N. W., and Bell, A. T., *J. Catal.* **73,** 257 (1982).
38. Yates, J. T., and Cavanagh, R. R., *J. Catal.* **74,** 97 (1982).
39. Agrawal, P. K., Katzer, J. R., and Manogue, W. H., *J. Catal.* **74,** 332 (1982).
40. Polizzotti, R. S., and Schwarz, J. A., *J. Catal.* **77,** 1 (1982).
41. Novak, S., Madon, R. J., and Suhl, H., *J. Catal.* **77,** 141 (1982).
42. Baker, J. A., and Bell, A. T., *J. Catal.* **78,** 165 (1982).
43. Kobori, Y., Yamasaki, H., Naito, S., Onishi, T., and Tamaru, K., *J. Chem. Soc., Faraday Trans. 1,* **78,** 1473 (1982).
44. Mori, T., Masuda, H., Imai, H., Miyamoto, A., Baba, S., and Murakami, Y., *J. Phys. Chem.* **86,** 2753 (1982).
45. Wang, C. J., and Ekerdt, J. G., *J. Catal.* **80,** 172 (1983).
46. McCandlish, L. E., *J. Catal.* **83,** 362 (1983).
47. Dalmon, J. A., and Martin, G. A., *J. Catal.* **84,** 45 (1983).
48. Otarod, M., Ozawa, S., Yin, F., Chew, M., Cheh, H. Y., and Happel, J., *J. Catal.* **84,** 156 (1983).
49. Erley, W., McBreen, P. H., and Ibach, H., *J. Catal.* **84,** 229 (1983).
50. Rostrup-Nielsen, J. R., Pedersen, K., *J. Catal.* **59,** 395 (1979).
51. Dalmon, J. A., Martin, G. A., "Proceedings, 7th International Congress on Catalysis, Tokyo, 1980," p. 402. Kodansha/Elsevier, Tokyo/Amsterdam, 1981.
52. Romanowski, W., *Surf. Sci.* **18,** 373 (1969).